

Dynamics of multiply charged ions in intense laser fields

S. X. Hu* and C. H. Keitel†

Theoretische Quantendynamik, Fakultät für Physik, Albert-Ludwigs-Universität Freiburg, Hermann-Herder-Straße 3, D-79104 Freiburg, Germany

(Received 3 May 2000; published 10 April 2001)

We numerically investigate the dynamics of multiply charged hydrogenic ions in near-optical linearly polarized laser fields with intensities of order 10^{16} – 10^{17} W/cm². The weakly relativistic interaction is appropriately described by the Hamiltonian arising from the expansion of the Dirac equation up to the second order in the ratio of the electron velocity v and the speed of light c . Depending on the charge state Z of the ion, the relation of strength between laser field and ionic core changes. We find around $Z=12$, typical multiphoton dynamics and for $Z=3$ tunneling behavior, however, with clear relativistic signatures. In first order in v/c the magnetic field component of the laser field induces a Z dependent drift in the laser propagation direction and a substantial Z dependent angular momentum with respect to the ionic core. While spin oscillations occur already in first order in v/c as described by the Pauli equation, spin induced forces via spin-orbit coupling only appear in the parameter regime where $(v/c)^2$ corrections are significant. In this regime for $Z=12$ ions, we show strong splittings of resonant spectral lines due to spin-orbit coupling and substantial corrections to the conventional Stark shift due to the relativistic mass shift while those to the Darwin term are shown to be small. For smaller charges or higher laser intensities, parts of the electronic wave packet may tunnel through the potential barrier of the ionic core and when recombining, are shown to give rise to keV harmonics in the radiation spectrum. Some parts of the wave packet do not recombine after ionization and we find very energetic electrons in the weakly relativistic regime of above threshold ionization.

DOI: 10.1103/PhysRevA.63.053402

PACS number(s): 32.80.Rm, 42.50.Hz, 33.40.+f

I. INTRODUCTION

Various techniques to generate ultrashort pulses such as chirped-pulse amplification [1] have been developed and perfected over the last years such that nowadays powerful laser pulses are available over a wide range of frequencies and pulse lengths up to intensities of 10^{21} W/cm² [2]. For intensities of 10^{16} W/cm²– 10^{19} W/cm², the electric field strength of the laser pulse is already comparable up to far stronger than the atomic unit field strength ($\sim 5.14 \times 10^9$ V/cm) that is experienced by an electron on the first Bohr orbit of hydrogen and in fact those fields are already accessible in quite numerous laboratories worldwide in rather small tabletop setups.

Especially for laser intensities till at about 10^{16} W/cm² there has been a lot of activity over the last two decades in intense nonrelativistic laser interactions with matter including atoms [3], molecules [4], clusters [5], and solids [6]. Many highly nonlinear optical phenomena such as high-order harmonic generation [7–10] above-threshold ionization (ATI) [11] and for higher frequencies and intensities stabilization [12], have attracted much attention for both experimentalists and theorists. Since optical laser fields of intensity 10^{21} W/cm² have become available in a rather short time, both theoretical and experimental activities moved quite quickly into the regime of fully relativistic dynamics up to around 10^{18} W/cm²– 10^{22} W/cm² [13–15] with experimental

emphasis on free electron dynamics, QED effects, and nuclear reaction processes [16,17]. There has been rather little activity, however, for neutral atoms interacting with optical laser fields of intensity 10^{16} W/cm²– 10^{17} W/cm² merely for the reason that there is almost instantaneous ionization for those intensities and the free electron dynamics is quite well understood for a long time [18]. For higher frequencies, ionization may be retained at those intensities, however, will also occur eventually for larger laser intensities due to the magnetic drift [13] with a likelihood for magnetic recollisions being usually smaller than that in the laser polarization direction [19].

For an ionic system one may have the unique possibility to apply relativistic near-optical laser field pulses and still allow for bound dynamics. The physical processes occurring will not merely scale with the ionic charge but be fundamentally different because of relativity and later QED governing the dynamics. Nowadays, ions may be processed from essentially all existing atoms with arbitrary charge state, absolute purity, and quite high density by sending them through foils [20] while due to lasers high charge states have also been achieved as well, however, with limits in the width of the charge distribution and the absolute charge [21]. The mean electric field sensed by a ground state electron of hydrogenic uranium corresponds to 1.8×10^{16} V/cm. Thus laser fields that are comparable in strength need have an intensity of order 10^{29} W/cm² and are thus far beyond reach nowadays. For those intensities, the dynamics will be absolutely remote from that of hydrogen with, say, a laser field of 10^{14} W/cm² and we do not aim to make the corresponding comparison in this paper. We consider it, however, more interesting to carry out a comparison of the nonrelativistic laser atom interaction with the weakly relativistic dynamics of an ion of

*Present address: Department of Physics and Astronomy, University of Nebraska–Lincoln, Lincoln, NE 68588-0111. Email address: shu@unlnotes.unl.edu

†Email address: keitel@physik.uni-freiburg.de

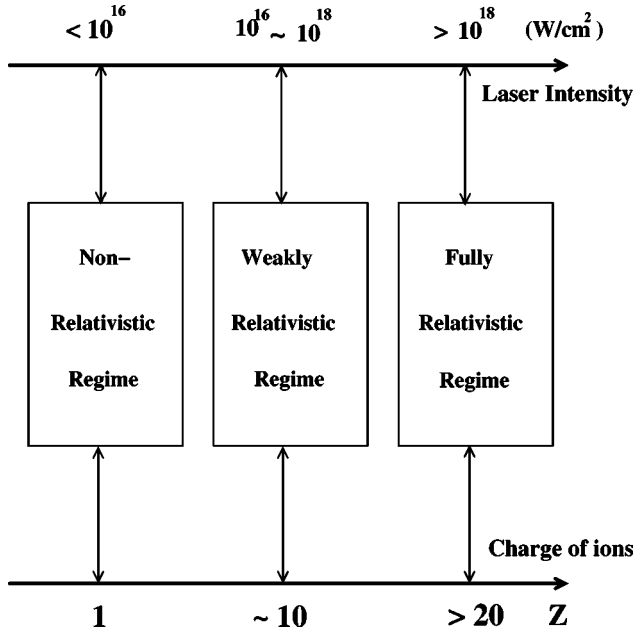


FIG. 1. Schematic sketch relating near-optical laser intensities to the charge state Z of a single electron ion such that the laser electric field and that of the nucleus become comparable, i.e., the laser field induces a nonperturbative interaction without large ionization. The emphasis of this paper is on the weakly relativistic regime from $Z = 3$ to $Z = 12$.

charge around 10 with laser fields of intensity 10^{16} W/cm²– 10^{17} W/cm² (see Fig. 1). Here relativity induces merely corrections and it is possible to identify the leading deviations to nonrelativistic dynamics as that of the laser magnetic field component, the breakdown of the dipole approximation, spin-orbit coupling, zitterbewegung, and the relativistic mass shift. In earlier letters we have shown that the magnetic field component of the laser pulse induces an enhanced angular momentum and thus a reduced electron expectation value in the vicinity of the multiply charged ion [22] and the existence of spin signatures in bound electron dynamics and radiation [23].

In terms of applications, multiply charged ions in relativistic laser fields appear also attractive for the generation of energetic electrons and high harmonics. The kinetic energy of a laser-accelerated electron as characterized by the parameter U_p does certainly increase with rising laser intensity. For harmonic generation especially, it is necessary that the highly energetic electron interacts periodically with the nucleus, urging us to enhance the charge of the ionic core, i.e., the ionization potential I_p correspondingly. As long as tunneling and recollisions can be assured with an appropriate relation of U_p and I_p , the simultaneous increase of both parameters is obviously attractive as the cut-off energy of high harmonic generation is given by the sum of I_p and the maximal kinetic energy at the time of recollision being of order U_p .

In this paper, we study the dynamics of multiply charged ions in intense laser fields in the weakly relativistic parameter regime where terms up to $1/c^2$ are still of significance and higher terms become negligible. For this purpose we

solve numerically the two-dimensional time-dependent expansion of the Dirac equation, which is exact up to all orders in $1/c^2$ and, which was first derived by Foldy and Wouthuysen [24]. Different weakly relativistic effects arise and we can investigate each by solving the dynamics and comparing the situations in which we include or neglect the corresponding part of the Hamiltonian associated with the effect of interest. As a function of the ionic charge relative to the laser field intensity, the electric and magnetic field components of the laser field will be shown to be either strong enough to lead to ionization in the polarization and propagation directions or give rise to interesting structures in the near vicinity of the ionic core. We point out the role of the spin in inducing stronger binding of the electronic wave packet and multiphoton spectral line splitting due to spin-orbit coupling. This is compared with the situation via the Pauli equation where spin induced forces are neglected. We further show that the relativistic mass shift induces a significant shift of especially the highly excited eigenenergies of the ion with respect to the conventional Stark shift and point out the consequences for the spectral lines. For relatively high intensities, special emphasis is placed on the tunneling regime in the weakly relativistic regime. For multiply charged ions, we find that both tunneling and recollisions are still possible and indicate harmonic generation in the keV regime. We note, however, that the plateau of the harmonic spectrum, well known in the nonrelativistic regime, is tilted increasingly in the relativistic regime with rising charge. This deviation to conventional high harmonic spectra is not too surprising as an electric wave packet attempting to recollide due to a phase shift of the electric field in the laser polarization direction may still partly or totally miss the ionic core due the magnetic drift in the laser propagation direction, especially for long recollision times. In the above threshold spectra we find high electron energies in the keV regime that are separated by the photon energy of the applied laser field.

This paper is arranged as follows: In Sec. II, we derive the Hamiltonian of interest along the lines of Foldy and Wouthuysen, then describe the numerical methods for solving the corresponding dynamical equation and present the details for computing the observable quantities of interest. In Sec. III A we then present effects up to first order in $1/c$ as those induced by the magnetic field component of the laser field. In Sec. III B we investigate the relativistic corrections to the Stark shift for laser-driven ions followed by a study of spin induced forces and the consequent splitting of spectral features in Sec. III C. Subsequently, relativistic high order harmonic generation is discussed in Sec. III D as well as the photoelectron spectra in Sec. III E. Finally, a conclusion is drawn.

II. PRELIMINARY CONSIDERATIONS

In this more technical section we present subsequently the Hamiltonian describing our system of interest, explain how we solve the corresponding dynamical equation numerically via the split-step mechanism, and finally quantify the observables to be investigated in the following section.

A. System and Hamiltonian

We are interested throughout this article in the dynamics of multiply charged ions of charge state up to $Z=12$ with moderate laser intensities (10^{16} – 10^{17} W/cm²) and near optical frequencies for the KrF (248 nm; 0.1838 a.u.) laser system and the doubled Nd:glass laser frequency (527 nm; 0.0866 a.u.). The maximum velocity of electron wave packets reaches the order $v=0.1c$, where $c=137.036$ denotes the speed of light in atomic units. We are therefore entitled to consider the Dirac equation up to second order in v/c and have confirmed that for our parameters, high order corrections do not play a role. One may derive this Hamiltonian via various unitary transformations along the lines of the Foldy-Wouthuysen (FW) expansion [24] of the Dirac equation or alternatively, without significant deviations, find the first-order relativistic corrections to the Pauli equation [25]. As opposed to nonrelativistic treatments, we need to include at least two dimensions in the calculation as the magnetic field component of the laser pulse may induce a significant drift in the laser propagation direction. There is a spin-induced force in the magnetic field direction [26], i.e., in the remaining third dimension, but the influence is small for the observables and the parameters of interest here.

Our working Hamiltonian \mathbf{H}_{FW} involves a series of relativistic corrections to the usual nonrelativistic Schrödinger Hamiltonian. One well-known correction term in v/c to the Schrödinger equation is the additional term in the Pauli equation representing the coupling of the laser magnetic field to the spin degree of freedom of the electron wave packet. The second-order terms include the spin-orbit coupling, i.e., the feed-back of the oscillating spin to the electron motion as well as the leading relativistic mass shift term and Zitterbewegung. The terms of order $O(1/c^3)$ do not play a role for the parameters employed though it would certainly be necessary to include them for the fully relativistic regime involving more intense laser fields and higher charged ions. The main advantage of using this equation in comparison to the full Dirac equation is the possible isolation of the influence of each physical mechanism arising. In addition, this equation does not limit us numerically to use high frequency lasers as necessary so far with the full Dirac equation [15].

For the circumstances with laser parameters described above, the FW Hamiltonian (2×2 matrix) of a bound electron in a strong laser field can be written (in atomic units) as

$$\begin{aligned}\mathbf{H}_{\text{FW}} &= \mathbf{H}_0 + \mathbf{H}_{\text{P}} + \mathbf{H}_{\text{kin}} + \mathbf{H}_{\text{D}} + \mathbf{H}_{\text{so}}, \\ \mathbf{H}_0 &= \{\mathbf{p} + \mathbf{A}(z,t)/c\}^2/2 + V(x,z), \\ \mathbf{H}_{\text{P}} &= \boldsymbol{\sigma} \cdot \mathbf{B}(z,t)/2c, \\ \mathbf{H}_{\text{kin}} &= -\mathbf{p}^4/8c^2, \\ \mathbf{H}_{\text{D}} &= \text{div } \mathbf{E}'(x,z,t)/8c^2, \\ \mathbf{H}_{\text{so}} &= i\boldsymbol{\sigma} \cdot \text{curl } \mathbf{E}'/8c^2 + \boldsymbol{\sigma} \cdot \mathbf{E}' \times \mathbf{p}/4c^2.\end{aligned}\tag{1}$$

Here \mathbf{H}_0 denotes the standard nonrelativistic Hamiltonian in Schrödinger form where $\mathbf{p}=(p_x,0,p_z)=(-i\partial/\partial x,0,$

$-i\partial/\partial z)$ is the two-dimensional momentum operator and $\mathbf{A}(z,t)$ is the time-spatial dependent vector potential of the laser field $\mathbf{E}(z,t)$, which is linearly polarized along the x axis and propagates in z direction. For the vector potential, we include the magnetic field component and do not apply the dipole approximation, urging us to perform a two-dimensional numerical integration in the x - z plane. Since \mathbf{H}_0 and all other Hamiltonians are 2×2 matrices, they need be considered as multiplied by the unity matrix \mathbf{I} even if not shown explicitly throughout this paper. We consider multiply charged ions in the single active electron approximation [27], which are preionized by several or more than ten electrons and thus are easily available today via lasers [21] or with highest accuracy via shooting the atoms through thin foiles [20]. Those are well described by the soft-core potential [28] to model the Coulomb field experienced by the active electron of a multiply charged ion, i.e.,

$$V(x,z) = -k/\sqrt{q_e + x^2 + z^2}.\tag{2}$$

The parameter k is a function of the effective number of positive charges Z as sensed by the electron. q_e compensates for the effect of possible inner electrons and reduced distances of the electronic wave packet to the ionic core in two- rather than three-dimensional calculations. k may be adapted such that we obtain the correct ionization energy for the system of interest with effective charge of the ionic core Z and charge of the ion $Z-1$. The static field of the ionic core is expressed by the gradient of the potential $-\nabla V(x,z)$ and $\mathbf{E}'(x,z,t)$ stands for the sum of this field plus the laser field $\mathbf{E}(z,t)$. The following term \mathbf{H}_{P} in Eq. (1) indicates the coupling of the laser magnetic field \mathbf{B} to the electronic spin as described by the Pauli matrix $\boldsymbol{\sigma}$. The sum $\mathbf{H}_0 + \mathbf{H}_{\text{P}}$ leads to the Hamiltonian in the well known Pauli equation. Further, in Eq. (1) \mathbf{H}_{kin} denotes the leading term for the relativistic mass increase and \mathbf{H}_{D} is the well-known Darwin term. Finally, the last term in the Hamiltonian \mathbf{H}_{so} stands for the spin-orbit coupling. Considering our central potential $V(x,z)$, the first term of \mathbf{H}_{so} in Eq. (1) disappears because $\nabla \times [-\nabla V(x,z)] = 0$ and the contribution due to the laser field is of order $1/c^3$. Thus, the spin-orbit coupling term becomes

$$\mathbf{H}_{\text{so}} = \boldsymbol{\sigma} \cdot \mathbf{E}' \times \mathbf{p}/4c^2 = \boldsymbol{\sigma} \cdot \mathbf{E} \times \mathbf{p}/4c^2 + f(x,z)\boldsymbol{\sigma} \cdot \mathbf{L}\tag{3}$$

with $f(x,z) = -k(q_e + x^2 + z^2)^{-3/2}/4c^2$ and where $\mathbf{L} = \mathbf{r} \times \mathbf{p} = (0, zp_x - xp_z, 0)$ is the orbital angular momentum of which only the component along the y direction is nonzero. The origin of spin-orbit coupling can alternatively be viewed also as being due to the interaction between the magnetic moment of the electron and the magnetic field \mathbf{B}' due to the motion of the positively charged core as sensed by the electron in its own rest frame.

B. Dynamics and numerical approach

We investigate the dynamics of multiply charged ions exposed to an intense laser field through solving the following dynamical equation, involving the previously derived Hamil-

tonian \mathbf{H}_{FW} in Eq. (1) (for convenience, we use the usual atomic units throughout this paper),

$$i\frac{\partial}{\partial t}\begin{pmatrix} \Psi_{up}(x,z,t) \\ \Psi_{down}(x,z,t) \end{pmatrix} = \mathbf{H}_{\text{FW}}\begin{pmatrix} \Psi_{up}(x,z,t) \\ \Psi_{down}(x,z,t) \end{pmatrix}. \quad (4)$$

The wave function has two components corresponding to spin-up and spin-down polarization of the electron and \mathbf{H}_{FW} is consequently a 2×2 matrix operator. The coupling to negative energy states as included in conventional Dirac theory is negligible in second order in v/c . The laser field is

assumed to be linearly polarized along the x axis so that the vector potential $\mathbf{A}(z,t)$ of the laser field may be of the form

$$\mathbf{A}(z,t) = (A_x(z,t), 0, 0), \quad (5)$$

where the z dependence of the vector potential reflects the propagation of the laser pulse in the z direction. The spatial dependence of the vector potential indicates that the magnetic component of the laser field $B = \nabla \times \mathbf{A}(z,t)/c \neq 0$ is included and we do not (and cannot) carry out the dipole approximation. We choose the vector potential $A_x(z,t)$ to be

$$A_x(z,t) = \begin{cases} -\frac{cE_0}{\omega t_{on}} \left[(t-z/c)\sin(\omega t - \omega z/c) + \frac{1}{\omega} \cos(\omega t - \omega z/c) \right], & 0 < t-z/c \leq t_{on} \\ -\frac{cE_0}{\omega} \sin(\omega t - \omega z/c), & t_{on} < t-z/c < t_p, \end{cases} \quad (6)$$

which is associated with a linearly polarized laser field with electric field E_x and magnetic field B_y components

$$E_x(z,t) = B_y(z,t) = \begin{cases} E_0 \frac{t-z/c}{t_{on}} \cos(\omega t - \omega z/c), & 0 < t-z/c \leq t_{on} \\ E_0 \cos(\omega t - \omega z/c), & t_{on} < t-z/c < t_p \end{cases} \quad (7)$$

being oriented in the x and y direction, respectively, and propagating both in phase in the z direction. Here, E_0 and ω are the maximal amplitudes of both fields and the angular frequency of the laser field, respectively. Further t_{on} is associated with the linear rising time of the laser pulse, i.e., 0 is the beginning of the turn-on and t_{on} the end of it. We note that the vector potential, Eq. (6), may not be continuous at the end of the turn-on phase, however, it is when t_{on} is chosen such that $\omega(t_{on} - z/c) = (m + 0.25)2\pi$ with m being an arbitrary integer. The measurable electric field strength, however, is always continuous. After the turn-on phase the pulse is assumed to have a constant amplitude till time t_p . Obviously a realistic pulse will turn off afterwards smoothly, however, for all observables of interest here this phase is of no interest and numerical calculations usually terminate at t_p .

Since the laser field is linearly polarized, the interaction term involves a term of the form $\mathbf{p} \cdot \mathbf{A}(\mathbf{z}, t)/c = p_x A_x(z, t)/c$, which means no coupling between momentum and coordinate space. This is because the term couples only the x component of the momentum with a function, which is dependent on z but not on x . Thus, we can still apply the usual split-operator algorithm [29] to solve the two-dimensional time-dependent matrix equation (4) via

$$\begin{pmatrix} \Psi_{up}(x,z,t+\Delta t) \\ \Psi_{down}(x,z,t+\Delta t) \end{pmatrix} = \exp[-i\Delta t\{p^2/4 - p^4/(16c^2)\}\mathbf{I}] \\ \times \exp[-i\Delta t\{\mathbf{p} \cdot \mathbf{A}/c + A^2/c^2 \\ + V(x,z) + \mathbf{H}_D\}\mathbf{I}] \\ \times \exp[-i\Delta t(\mathbf{H}_P + \mathbf{H}_{so})] \\ \times \exp[-i\Delta t\{p^2/4 - p^4/(16c^2)\}\mathbf{I}] \\ \times \begin{pmatrix} \Psi_{up}(x,z,t) \\ \Psi_{down}(x,z,t) \end{pmatrix}. \quad (8)$$

Here Δt denotes the time step and the unit matrix operator is described with \mathbf{I} . All exponential operators except the term $\exp[-i\Delta t(\mathbf{H}_P + \mathbf{H}_{so})]$ are diagonal and we apply the split evolution operator on the wave function with the help of Fourier transform between the coordinate representation and the momentum representation. Consequently all derivative operator can be transformed into multiplications with constants. For nondiagonal exponential operators, we usually need to diagonalize them. Fortunately, the nondiagonal operator $\exp[-i\Delta t(H_P + H_{so})]$ involved here only depends on the specific Pauli matrix σ so that we can carry out the Taylor expansion for this exponential operator up to the order of interest here. The operators may be split in the way given because commutators of order $O([\Delta t]^3)$ and $1/c^3$ are negligible here. Regarding the interaction term $p_x A_x/c$, special care is needed as mentioned above. Here we do the Fourier transformation only for the x coordinate because of the z coordinate dependence of the vector potential $A_x(z,t)$. This, however, is sufficient and the exponential function of operators of interaction terms on the wave function ends up being merely a sequence of Fourier transformations and c -number multiplications. Because of the splitting of the total Hamiltonian in the exponent, we introduce an error following the

Baker-Hausdorff formula because the split terms generally do not commute. The error of this algorithm is of order $(\Delta t)^3$ between every successive time step. Thus, a small time step can ensure to get accurate results, and we have not experienced any problem with numerical convergence in the regime of interest here.

From the numerical point of view, we first solve for the eigenstates of the bound electron in the ionic core potential by using the so-called ‘‘spectral’’ method [30]. In fact, we choose a testing wave function without any symmetries to propagate on the two-dimensional potential. This way we obtain all symmetric and asymmetric eigenstates of the system. As an example, Fig. 2 shows the energy-level structure of a model hydrogenlike ion Mg^{11+} of which the single active electron experiences the nucleus with charges $Z=12$. Choosing $k=80.32$ and $q_e=1.0$, we get the corresponding ground-state energy -72 a.u. Note that it is not our purpose to present an exact quantitative model of the ionic level structure of an ionic system. We model single-electron ions with a softcore rather than a Coulomb potential and can adapt the ground state energy by choosing k and q_e . With the assumption of a smoothing around the ionic core, we deviate from the exact Coulombic potential and the system may also be considered as an active electron plus an ionic core where lower shells are filled and inactive. In the intensity range where level structures are important we thus can only make qualitative statements for the dynamics if we want to associate it with a particular realistic ion. In the tunneling regime, however, where structure becomes less important and only the correct ground state is significant we can be quantitative as well.

The ground-state wave packet of our model ion relates to a symmetric s -state wave packet, and also the second excited-state wave packet [see Fig. 2(b)]. The first, third, and fourth excited states are asymmetric (especially non s states) in space. This system will be applied to evaluate the relativistic Stark shift in Sec. III B. After obtaining the eigenstates $\Phi_n(x, z)$, we may use the above split-step operator in Eq. (8) to investigate the evolution of multiply charged ions under the irradiation of external intense lasers. When the laser pulse is turned on, the system is assumed to evolve from the spin-polarized ground state, that is, the initial condition $\Psi_{up}(x, z, t=0) = \Phi_1(x, z)$ and $\Psi_{down}(x, z, t=0) = 0$.

C. Observables of interest

With the knowledge of the time-dependent wave function, we are in a position to calculate the spatial probability distribution $|\Psi(x, z, t)|^2 = |\Psi_{up}(x, z, t)|^2 + |\Psi_{down}(x, z, t)|^2$ and the expectation value of any observable \mathcal{O} associated with the system via

$$\langle \mathcal{O}(t) \rangle = \int_{x_{min}}^{x_{max}} dx \int_{z_{min}}^{z_{max}} dz (\Psi_{up}(x, z, t), \Psi_{down}(x, z, t)) \times \mathcal{O}(x, z, t) \begin{pmatrix} \Psi_{up}(x, z, t) \\ \Psi_{down}(x, z, t) \end{pmatrix}. \quad (9)$$

Here the integral turns into a sum in our case as the wave

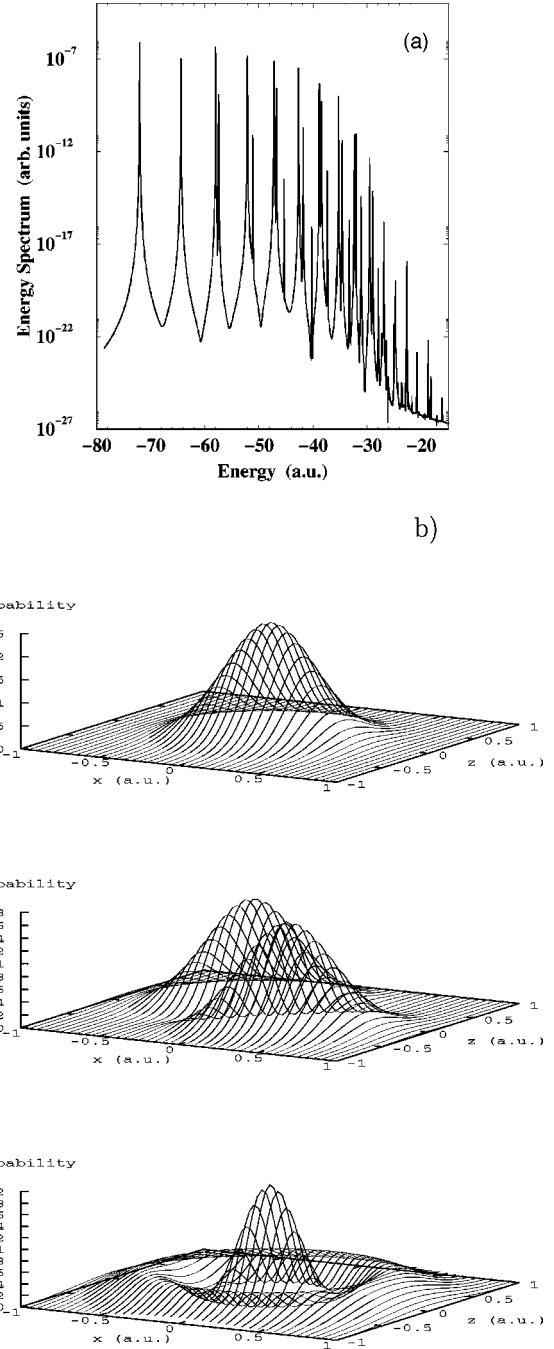


FIG. 2. (a) The energy-level structure of a model multiply charged ion with $Z=12$. The potential is described by a soft-core model $-k/\sqrt{q_e+x^2+z^2}$ with $k=80.32$ and $q_e=1.0$ and ground state energy of -72 a.u. (b) The probability distributions of the electronic wave packets for our model multiply charged ion for the three lowest energy states $|g\rangle$, $|1e\rangle$, and $|2e\rangle$, respectively, from the top to the bottom.

function is given on an equidistant grid from x_{min} to x_{max} in the polarization direction and from z_{min} to z_{max} in the propagation direction.

Particular interest in this article is placed on the spatial average values $\langle x(t)\mathbf{I} \rangle$ and $\langle z(t)\mathbf{I} \rangle$ of the wave packet and because of their relevance for the radiation spectrum on the

accelerations in the polarization direction $a_x(t) = \langle \ddot{x}(t) \mathbf{I} \rangle$ and in the propagation direction $a_z(t) = \langle \ddot{z}(t) \mathbf{I} \rangle$ via Eq. (9).

The radiation spectrum is generally given by a rather complex function of the accelerations and velocities in all spatial directions (see, e.g., Eq. 10.7 in the first review in [3]). For simplicity, we here restrict ourselves to an observation direction perpendicular to the $2d$ plane of motion, i.e., the y direction. Also, we are mostly interested in the dominating part of the radiation spectrum in the weakly relativistic regime, which is polarized in the polarization direction of the laser field. In the far field spectrum this is proportional to the squared Fourier transform of simply the acceleration $a_x(t) = \langle \ddot{x}(t) \mathbf{I} \rangle$. Also for the purpose of studying weakly relativistic signatures of the spectra, it is interesting to study the less intense spectrum, which is polarized in the laser propagation direction and governed by $a_z(t) = \langle \ddot{z}(t) \mathbf{I} \rangle$.

Under the assumption of including relativistic corrections up to second order in v/c , it is not sufficient for $a_x(t)$ to consider the gradient of the potential only as in the nonrelativistic regime. We rather find in the weakly relativistic limit

$$\begin{aligned} \ddot{x} &= \sqrt{1 - \dot{x}^2/c^2 - \dot{z}^2/c^2} \left\{ -\frac{\partial V(x,z)}{\partial x} + \frac{\dot{x}}{c} \left(\frac{\dot{x}}{c} \frac{\partial V(x,z)}{\partial x} \right. \right. \\ &\quad \left. \left. + \frac{\dot{z}}{c} \frac{\partial V(x,z)}{\partial z} \right) \right\} \\ &= \left(1 + \frac{3}{2c^2} \frac{\partial^2}{\partial x^2} + \frac{3}{2c^2} \frac{\partial^2}{\partial z^2} + O(1/c^4) \right) \left(-\frac{\partial V(x,z)}{\partial x} \right) \end{aligned} \quad (10)$$

$$\ddot{z} = \left(1 + \frac{3}{2c^2} \frac{\partial^2}{\partial x^2} + \frac{3}{2c^2} \frac{\partial^2}{\partial z^2} + O(1/c^4) \right) \left(-\frac{\partial V(x,z)}{\partial z} \right),$$

where for the transformation to the second part of the equation we substituted the time derivatives via $dx/dt = dH_{FW}/dp_x$ and $dz/dt = dH_{FW}/dp_z$ and will neglect the higher order terms in $O(1/c^4)$. We note that the first term in the right-hand side is just the nonrelativistic limit, and the following two terms correspond to weakly relativistic corrections that will be retained for the calculation of spectra. For the evaluation of the spectrum of interest, the operators in Eq. (10) need just be inserted in Eq. (9) and then to be Fourier transformed.

We now turn to the technical aspects for the evaluation of the photoelectron spectra. Since the expected ionization is equivalent to a proportion of the electronic wave function leaving the vicinity of the ionic core and propagating outwards towards the (unphysical) boundaries of the numerical grid, we must avoid reflections of the wave function at those boundaries. This is achieved by absorbing all parts of the wave function approaching the boundaries by a $\cos^{1/8}$ mask function [31], which results in a decrease of the norm of the wave function within the spatial box. While quite often only the part in the vicinity of the ionic core interests, it is here the opposite as we care only for the part of the wave function approaching the absorbing boundaries. Assume that we have calculated the wave packet dynamics up to time t_f in our finite box. Then we will have information about the photoelectron spectrum from what has been absorbed till this time at the boundaries at all intermediate times t_α and from the ionized part of the wave function still in the box. We begin by treating the absorbed electron flux, say, $\Psi_{flux}(x,z,t_\alpha)$ at time t_α after entering the area of the boundaries. As this part will certainly not be influenced by the ionic core, we will assume this to propagate to the end of interaction as a free particle (for details see [32]).

At the end of the interaction, at t_f , we also have to include the ionized part of the final spatial wave function still in the box. In order to obtain this from the full wave function it will be modified as follows, for example, for the spin-up part of the wave function

$$\Psi_{out}(x,z,t_f) = \begin{cases} 0, & |x| < X_I \\ \sin^2\{\pi(|x| - X_I)/2X_0\} \Psi_{up}(x,z,t_f), & X_I \leq |x| \leq X_I + X_0 \\ \Psi_{up}(x,z,t_f), & |x| > X_I + X_0. \end{cases} \quad (11)$$

Here X_I represents a range that may be related to the ionic radius within which the electron may be considered bound and we will ignore this part of the wave packet as we are only interested in the ionized part of the wave packet. We call X_0 the sliding range for the final wave function, where with increasing distance from the ionic core the wave function will contribute more to the photoelectron spectrum. Everything beyond $X_I + X_0$ can be considered as fully ionized and will fully contribute. The momentum wave function of

the ionized electron can then be obtained by fast Fourier transforming both the spatial wave function $\Psi_{out}(x,z,t_f)$ and the freely propagated $\Psi_{flux}(x,z,t_\alpha)$ with respect to x . We note that the main part of the electron distribution is ejected along the polarization direction in our range of parameters so that we focus here on the photoelectron spectrum in this direction even though it is analogous in the z direction. The momentum wave function describing the emitted electron distribution in x direction can be thus expressed as

$$\begin{aligned} \Psi_p(p_x, z, t_f) &= \mathcal{F}_x[\Psi_{out}(x, z, t_f)] \\ &+ \sum_{t_\alpha} \mathcal{F}_x[U^{(wv)}(t_f, t_\alpha) \Psi_{flux}(x, z, t_\alpha)]. \end{aligned} \quad (12)$$

Here the weakly relativistic Volkov propagator $U^{(wv)}(t_f, t_\alpha)$ is expressed as

$$\begin{aligned} U^{(wv)}(t_f, t_\alpha) &= 1/(2\pi)^3 \times \int d^3p \\ &\times \exp\left[-i \int_{t_\alpha}^{t_f} [\{p + A(\tau, z)\}^2/2 \right. \\ &\quad \left. - \{p + A(\tau, z)\}^4/8c^2] d\tau\right], \end{aligned}$$

which propagates the electronic wave packet absorbed at time t_α to the end of interaction time t_f . The symbol \mathcal{F}_x means fast Fourier transform of the wave function with respect to the x coordinate and p_x denotes the electron momentum along the x axis. The summation in the above equation is for all times t_α during which the absorbed part of the wave packet is detected. The kinetic energy spectrum of the photoelectron can then be obtained by integrating the momentum wave function over the z coordinate, i.e., $P(\epsilon_x, t_f) \approx (1 + \epsilon_x/c^2)/\sqrt{2\epsilon_x} \int \Psi_p(p_x, z, t_f) dz$. The prefactor has been derived via $dp_x/d\epsilon_x$ where the kinetic energy of the photoelectrons has been approximated via $\epsilon_x \approx p_x^2/2 - p_x^4/8c^2$ in atomic units including only weakly relativistic corrections in second order. The same procedure is carried out for the spin-down wave function and to obtain the total photoelectron spectrum, we sum over both polarizations.

III. RESULTS AND DISCUSSIONS

In this section we present and discuss the role of the magnetic laser component (Sec. III A) and of the relativistic mass effects (Sec. III B) on dynamics and radiation of laser driven ions. In (Sec. III C) spin effects are investigated regarding the Pauli $\sigma\mathbf{B}$ term that merely induces spin oscillations and the second order $\sigma\mathbf{L}$ term, which is responsible for spin induced forces. In (Sec. III D) harmonic generation is studied in the weakly relativistic regime and in (Sec. III E) highly energetic above threshold ionization.

A. Magnetic field effects

For neutral atoms interacting with moderately intense laser pulses, the magnetic component of the laser field can usually be ignored in the evaluation of the wave packet dynamics. Once, however, the velocity of the electron wave packet becomes non-negligible as compared to the velocity of light the Lorentz force $(\mathbf{v}/c) \times \mathbf{B}$ may not be ignored as compared to the electric field force of the laser field. This generally is the case when the relativity parameter $r = eE/(m\omega)$ is not negligible as compared to c , i.e., at least 1% depending on the observable of interest.

The magnetic field component of a linearly polarized laser field induces a drift in the laser propagation direction [18], that may be strong enough to induce instantaneous ionization even for high laser frequencies [13]. There is a regime, however, where the laser field and correspondingly the drift is weak enough such that the attraction of singly charged ions can still compensate for it and induce recollisions along the propagation direction [19]. If one does not want to be restricted in the laser field intensity, a more elegant solution to overcome the drift and avoid strong ionization would be to employ multiply charged ions.

In the following, we focus on the magnetic field (B field) induced time evolution of the electronic wave packet in the vicinity of and away from the ionic core, and since second-order relativistic effects turn out to be small for the employed laser and ion parameters, the Hamiltonian H_{FW} need only include the term H_0 . Thus, we numerically solve the two-dimensional time-dependent Schrödinger equation but beyond the usual dipole approximation and including the laser magnetic field, and the vector potential $A = A(z, t)$ consequently depends on both t and z .

In Fig. 3 we have displayed the dynamics of single-electron ions with charge $Z=3$ in (a) and $Z=4$ in (b) in a laser field with a wavelength of 248 nm and an intensity 1.2×10^{17} W/cm² during the pulse duration of 10-cycle constant amplitude. We have merely displayed the dynamics of the center of mass of the wave packet $[\langle x(t) \rangle, \langle z(t) \rangle]$ in order to compare with our classical intuition. For $Z=1$ and $Z=2$, we would have almost complete ionization for the laser intensity applied and the figure would resemble that of a classical-free electron drifting with its usual ‘‘zigzag’’ in the laser propagation direction [18]. For $Z=3$, we see in Fig. 3(a) that the ionic core starts to seriously compete with the drift imposed by the laser field, i.e., there is a substantial ionization in the laser polarization and propagation direction, however, also a significant part can still be kept close to the ionic core. Interesting to see is that parts of the wave packet may move opposite to the laser propagation direction similar to the magnetic recollisions advocated earlier [19]. We have also considered the center of mass motion restricted to a smaller area around the vicinity of the nucleus and found dynamics resembling the ‘‘figure of 8 motion’’ known in the frame where the drift is transformed away. Simulations of the full wave packet have confirmed the dynamics towards and away from the nucleus in the laser propagation direction and the significant amount of ionization.

A different situation occurs in Fig. 3(b) for $Z=4$ when the ion charge is high enough to avoid substantial ionization and to allow for weakly relativistic bound dynamics. The electronic wave packet will oscillate around the ionic core with a particularly high velocity in its close vicinity. At the times when the electronic wave packet approaches the ionic core, the magnetic field component also turns out to be large. Therefore, an extremely strong Lorentz push of the wave packet around the ionic core in the laser propagation direction arises and results in a low electron expectation value close to the ionic core [22]. The ‘‘open diamonds’’ represent the case without magnetic field, i.e., the situation within the dipole approximation. Here the electronic wave packet does

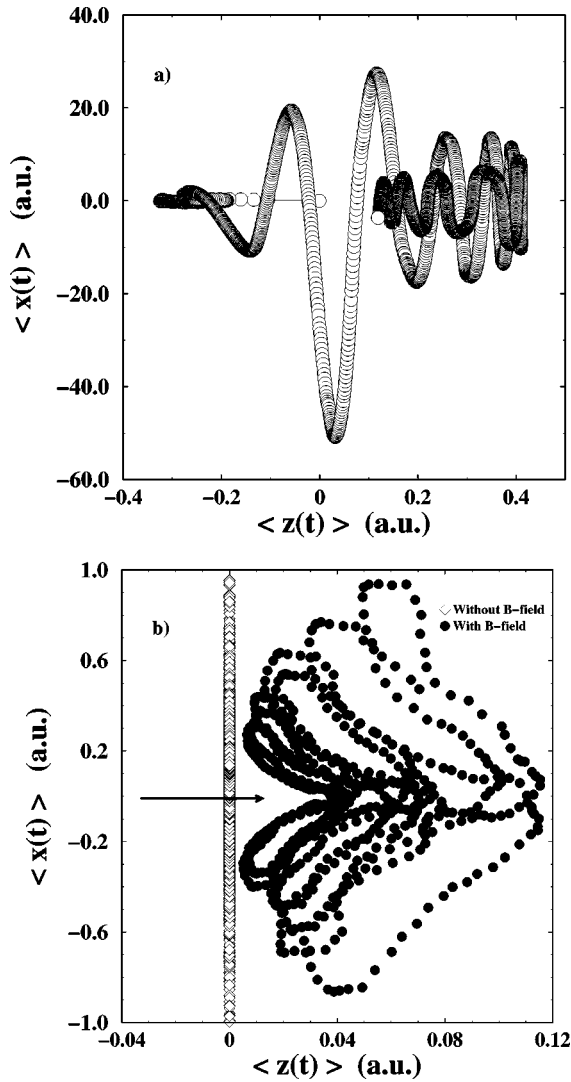


FIG. 3. The center-of-mass evolution of the electronic wave packet for the cases with B field [“open circles” in (a) and “full circles” in (b)] and without B field (“open diamonds”). The laser parameters involve a wavelength of 248 nm, an intensity of 1.2×10^{17} W/cm², a three-cycle linear turn-on and a ten-cycle constant amplitude duration. For Li²⁺ in a) ($Z=3$, $q_e=1.0$, $k=6.48$) there is a significant drift in the laser propagation direction and in addition to substantial ionization (not visible), a considerable part of the wave packet returns to the nucleus opposite to the laser propagation direction. A reduction of the expectation value of the electronic wave packet is observed around the close vicinity of the ionic core for Be³⁺ ($Z=4$, $q_e=1$, $k=10.7$) as indicated by the arrow in (b), when the B field is involved.

merely carry out one-dimensional oscillations along the laser polarization direction, i.e., along the x axis, as expected. However, when the magnetic component of the laser field is included in the calculation, the electronic wave packet is pushed towards the laser propagation direction (z axis) as visible from the full circles. This magnetically induced pressure on the electronic wave packet is significantly increased around the ionic core as seen in the Fig. 3(b). It results in a low electron probability in the vicinity of the ionic core. This can be interpreted as a hole around the nucleus at ($x=0, z$

$=0$) as indicated by the arrow in Fig. 3(b). Comparing with [22], we note that the size of the hole may increase with rising laser intensity. We need to emphasize that we do not put forward holes from knocking out complete inner-shell electrons from multielectron systems. We rather discuss the strong reduction of the wave packet expectation value of single active electrons near the nucleus. For a multielectron system, however, inner-shell electrons are likely to be more affected by the magnetically and ionic core induced Lorentz push investigated here simply because the attraction from the nucleus is even larger then.

It may be obvious that the electron velocity near the nucleus is high for multiply charged ions. However, we need explain why the magnetic field, also necessary for the Lorentz force, is significant at the time of the return of the electronic wave packet to the nucleus. When the electronic wave packet returns to the nucleus with essentially maximum velocity, the amplitude of the magnetic component of the laser field should become nearly zero. This is because velocity and force are generally phase shifted by $\pi/2$. However, due to the existence of the multiply charged ionic core and the increasing field intensity during the turn-on of the laser field, an important phase lag can be developed during the laser pulse turn-on, which is very critical for the hole formation around the ionic core. During the laser pulse turn-on, the electronic wave packet does not move like a quasifree particle because of the tight binding of the ionic core. When the electronic wave packet is dragged outwards by the laser force, the strong ionic core tries to attract it, which results in an important phase lag between the wave packet motion and the laser field. Usually, when the wave packet returns to the nucleus, this effect is again compensated because this time the ionic core accelerates the electric wave packet towards it. However, because of the increasing field in the turn-on phase of the laser pulse, the laser force is stronger then, the Coulomb force is comparably weaker, and the phase lag is consequently only partially compensated. Once the pulse is at full intensity, the phase lag remains almost unchanged till the field maximal amplitude begins to decrease again.

In the following, we investigate the electronic relaxation dynamics after the laser pulse arising from the reduced circular motion around the ionic core. For this purpose, we allow the “hollow” ion to evolve freely for a time period of 30 laser cycles after the laser-ion interaction and during this time observe its relaxation dynamics and radiation. We note that the hollowing out of the ion due to the magnetic field will be reversed step by step in space during the relaxation process. In Fig. 4(a) we have shown the component of the relaxation radiation in the laser polarization direction accompanying this process for the same potential and laser field parameters as in Fig. 3(b). Apparently, the reverse process to magnetically induce hollowing out of the ion gives rise to x-ray emission with distinct peaks up to ~ 230 eV photon energy. The main peak corresponds to the transition between the Stark-shifted first excited state $|1e\rangle$ and the ground state $|g\rangle$, as indicated in Fig. 4(b). Further the 122.67-eV peak is related to the transition $|4e\rangle \rightarrow |g\rangle$. In Fig. 4(c) we have displayed the same spectrum but with the component along the propagation direction of the laser field. This would be essen-

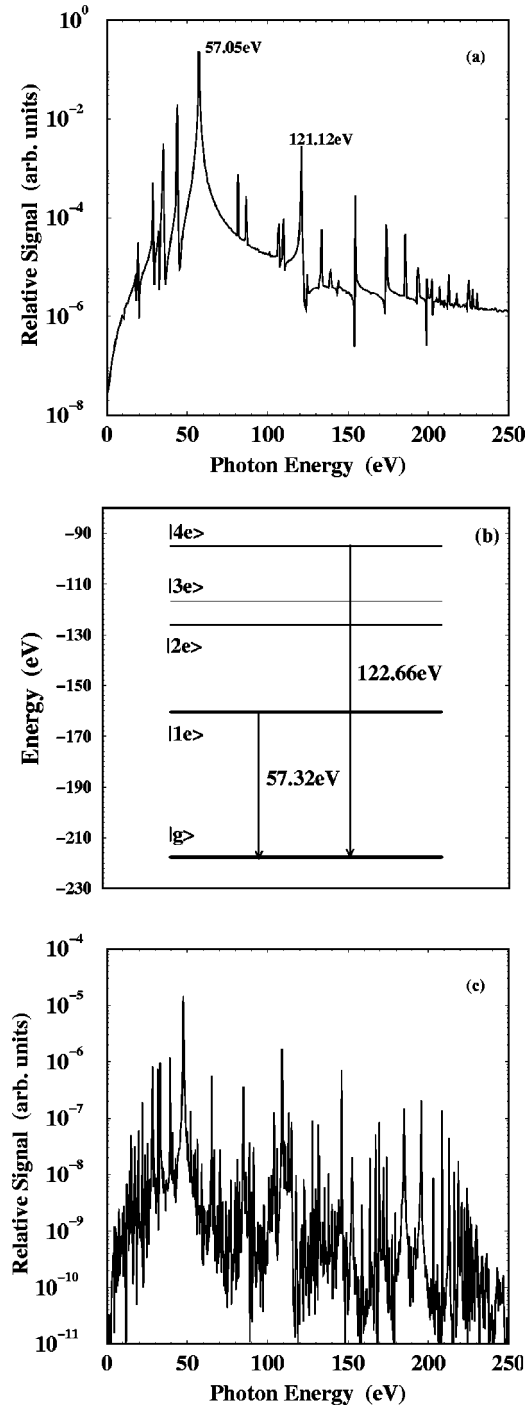


FIG. 4. (a) The relaxation radiation spectrum polarized in the laser polarization direction of the hollow ion [Be³⁺ as prepared for Fig. 3(b)] during the time of 30 laser cycles after the laser pulse. The strongly reduced expectation value close to the nucleus of the active electron is reversed again and x-ray radiation is emitted. The corresponding transitions are plotted in (b), which are modified by the Stark shift. (c) The corresponding radiation spectrum polarized in the laser propagation direction.

tially absent without the existence of the magnetic field component of the laser field that is inducing the dynamics in the laser propagation direction. Finally, we note that the hollowing out of the ion may be optimized by adjusting the inter-

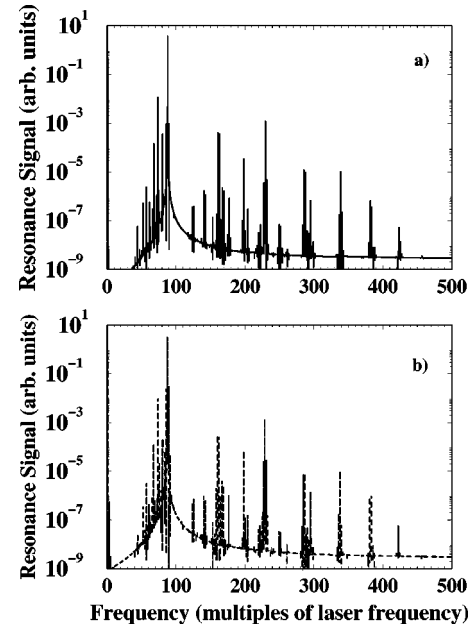


FIG. 5. The spectrum of $Z=12$ -model ions (with level structure indicated by Fig. 2), which are exposed to an intense laser pulse of intensity 7×10^{16} W/cm² and the laser wavelength 527 nm. The laser pulse has a 5.25-cycle turn-on, followed by a 100-cycle period with constant amplitude. The laser parameters are in the multiphoton regime with respect to the ion charge so that resonant structures are visible. The solid line in (a) and the dotted lines in (b) represent the cases without and with the leading relativistic correction, respectively.

action parameters such that the Lorentz force $\mathbf{v}/c \times \mathbf{B}$ becomes maximal near the nucleus.

B. Relativistic Stark shift

In this subsection, we investigate the role of relativistic corrections to the Stark shift as visible in the positions of the energy levels of intense laser driven ions. For this situation we choose the Hamiltonian $H_{FW} = H_0 + H_p + H_{kin}$. We find that the Pauli term has no notable effect on the shift of energy levels but we include it for the sake of inclusion of all first-order relativistic effects. The leading second-order term in the weakly relativistic regime is generally H_{kin} that may be associated with a relativistic mass increase. We note that the Darwin term is insignificant in its effect compared to the mass increase and in fact also to spin-orbit coupling. Since in this subsection we are not interested in line splitting but in the total shift of spectral components, we do not include H_{so} here. The effect of the mass increase in intense laser driven atoms has been discussed before and associated with an enhancement of stabilization [33] and with Doppler shifts of harmonics [34]. Here we focus however on the multiphoton regime and how the ionic bound energy levels are shifted in addition to the conventional Stark shift.

We choose the model $Z=12$ ion as described in Sec. II B as target. The laser parameters involved are the intensity 7×10^{16} W/cm², the wavelength 527 nm, and a pulse includ-

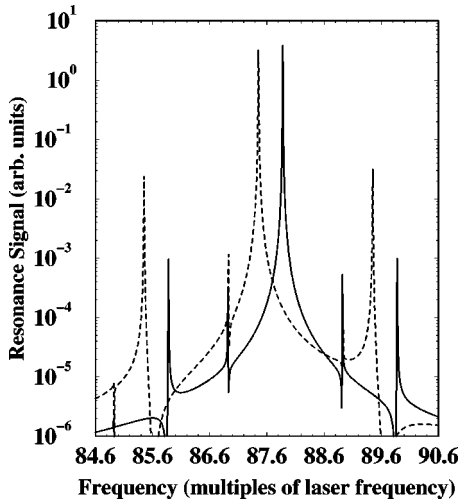


FIG. 6. The segment of Fig. 5 in the vicinity of the multiphoton resonance of the transition between the bound states $|1e\rangle \leftrightarrow |g\rangle$. The solid and dashed lines represent the cases without and with the leading relativistic corrections, respectively. A clear redshift of 0.43ω of the resonant line is observed when the leading relativistic corrections is taken into account. It can be attributed to the relativistic Stark shift of the energy levels of the ion.

ing a 5.25-cycle turn-on phase and 100 cycles with constant amplitude. The whole radiation spectrum is displayed in Fig. 5, in (a) without including H_{kin} in the full Hamiltonian and in (b) including it in the solution of the dynamical equation. The relativistic signatures are small on this scale, however, it is interesting to note that x rays via hundreds of photons of the applied laser frequency may be generated due to resonances in the multiphoton regime.

We note further numerous resonant structures due to multiphoton transitions among the ionic bound levels in addition to smaller peaks displaced by up to few photon energies of the applied laser field to the resonant lines. In order to have a clearer picture of the structure and the deviation due to the relativistic mass shift, we have depicted the enlargements of the first three dominant resonant spectral structures in Figs. 6, 7, and 8, respectively, for the multiphoton resonances of the ground state $|g\rangle$ to the first excited state $|1e\rangle$, to the second excited state $|2e\rangle$, and to the fourth excited state $|4e\rangle$. The third excited state $|3e\rangle$ resembles a d state and we find that the resonance on $|3e\rangle \leftrightarrow |g\rangle$ involves a coupling three orders of magnitude smaller than those of $|1e\rangle \leftrightarrow |g\rangle$ and $|4e\rangle \leftrightarrow |g\rangle$. We emphasize that our calculations are beyond the dipole approximation so that the usual selection rules do not apply. In these three figures the solid line and dashed line represent the cases in which relativistic corrections due to the mass shift are ignored and included, respectively.

In Fig. 6, we display the dominant resonant line, which is located at 87.88ω following the calculation without the relativistic mass shift correction. This corresponds to the energy difference between the ground state and the first excited state including the conventional nonrelativistic Stark shift. When the leading relativistic correction to the electron kinetic energy is taken into account, we find from the dashed line in

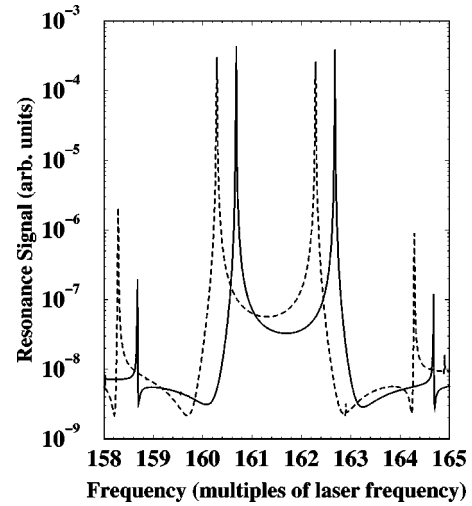


FIG. 7. Same as Fig. 6 but for the transition $|2e\rangle \leftrightarrow |g\rangle$. The redshift is up to 0.39ω for this case.

Fig. 6 the corresponding resonance shifts to 87.45ω with ω denoting the laser frequency. The additional redshift of the resonance transition of $|1e\rangle \leftrightarrow |g\rangle$ is as high as 0.43ω for the parameters chosen here. We refer to the correction as the ‘‘relativistic Stark shift.’’ Furthermore, we note clear peaks displaced by two laser photons to both sides of the main resonant lines; i.e., the laser stimulates the absorption or emission of two photons prior the emission of the high frequency photon from the resonant state. The effect of the relativistic Stark shift is clearly visible from the comparison of the dashed and solid line. In addition, small lines are visible that are displaced at about one-photon away from the resonances. Those would be forbidden under the dipole approximation, however, appear because of quadric and high-order contributions included in our calculation. Those are higher order terms and small in the weakly relativistic regime of interest here. Thus, higher-order corrections to the position of this small peak as by the relativistic Stark shift are even smaller and are not visible for this peak displayed

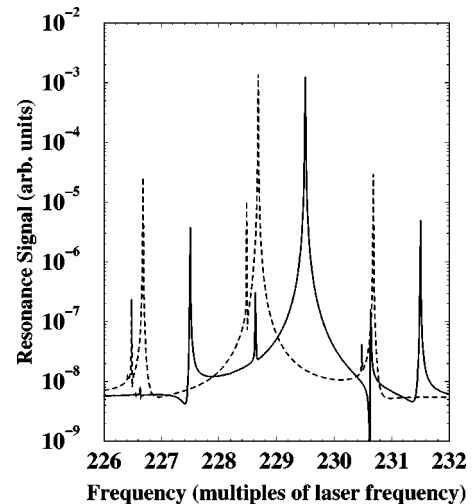


FIG. 8. Same as Fig. 6 but for the transition $|4e\rangle \leftrightarrow |g\rangle$. A large redshift of 0.82ω for the resonant transition is visible.

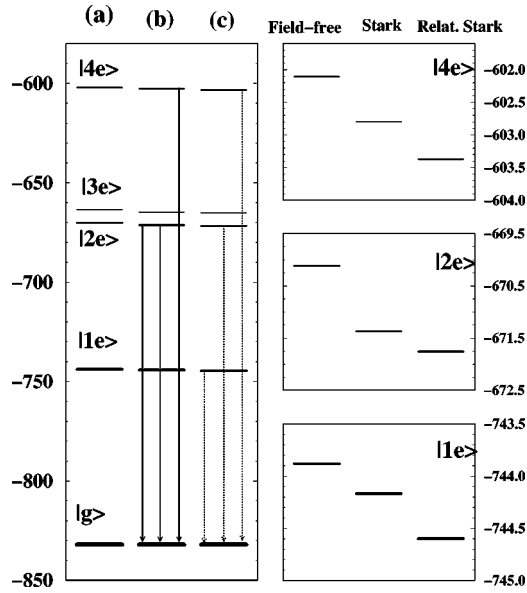


FIG. 9. Energy level diagram of the four lowest eigenstates of the $Z=12$ ion in an intense laser field as given in Fig. 5. In the left part, the column (a) shows the eigenstates without external fields, column (b) involves the conventional Stark shift, and the relativistic Stark shift is included in column (c). The transitions in columns (b) and (c) are corresponding to the solid and dotted lines in Figs. 6, 7, and 8. The details of the shifting process are enlarged in the right part for states $|1e\rangle$, $|2e\rangle$, and $|4e\rangle$.

by one photon around the $|1e\rangle \leftrightarrow |g\rangle$ transition. However, we note here already that it will be visible for higher excited states, for example, for the $|4e\rangle \leftrightarrow |g\rangle$ transition in Fig. 8.

For the resonance between $|2e\rangle \leftrightarrow |g\rangle$, the result is plotted in Fig. 7. It is similar to Fig. 6 but the relativistic Stark shift is only 0.39ω . As addressed in Sec. II B, the second excited state $|2e\rangle$ is symmetric in space and resembles an s state similar to the ground state $|g\rangle$ so that the resonant transition $|2e\rangle \leftrightarrow |g\rangle$ is considered. Thus only high order terms beyond the dipole term contribute. Considering the scale of the vertical axis, we find that the resonant signal is three orders of magnitude smaller than in the case for the $|1e\rangle \leftrightarrow |g\rangle$ transition. In addition, the relativistic Stark redshift turns out smaller than in the case of the $|1e\rangle \leftrightarrow |g\rangle$ resonance although the $|2e\rangle$ state is not so tightly bound as the state $|1e\rangle$. Moreover, the one-photon spaced peaks are no longer visible for the $|2e\rangle \leftrightarrow |g\rangle$ transition. If we continue to explore the $|4e\rangle \leftrightarrow |g\rangle$ resonance, we find that the relativistic Stark redshift becomes relatively large again, as indicated in Fig. 8. Since the state $|4e\rangle$ is asymmetric and resembles a p state as $|1e\rangle$, the dipole transition $|4e\rangle \leftrightarrow |g\rangle$ is permitted. Further, the state $|4e\rangle$ is less strongly bound by the ionic core and consequently much more easily influenced by the external field. Therefore, the relativistic Stark shift attains 0.82ω and is thus larger than in the cases for the transitions $|1e\rangle \leftrightarrow |g\rangle$ and $|2e\rangle \leftrightarrow |g\rangle$. Finally, the peaks spaced one photon away from the resonance appear again as already in Fig. 6, however, the relativistic Stark redshift becomes visible here also for these small peaks.

Figure 9 shows how the energy levels of the multiply

charged ion of interest move under the radiation of an intense laser field. In the left part, the column (a) represents the situation without laser field and the central part (b) indicates the inclusion of the usual Stark shift but without relativistic corrections. The column (c) includes the “relativistic Stark shift” in addition to the usual Stark shift, which arises from the leading relativistic correction to the kinetic energy of the electron. The detailed position of the states $|1e\rangle$, $|2e\rangle$, and $|4e\rangle$ is enlarged in the right part of Fig. 9. The series of transitions in columns (b) and (c) are corresponding to the solid lines and dotted lines in Figs. 6, 7 and 8, respectively. This figure gives us a clear picture of how the energy levels shift under an external intense laser field. The relativistic Stark shift, though small when compared to the absolute value of the energy levels, can clearly be identified in the radiation spectra and should, in principle, be measurable in experiments.

C. Spin effects

We now turn to the role of the spin degree of freedom of the electron in intense laser-ion interaction. In first order in v/c the Pauli equation already includes the coupling of the magnetic laser field to the spin as noted earlier [35]. We will not discuss this here and are more interested in the interaction of the spin degree of freedom with an operator describing the electron rather than the laser field. This is given by spin-orbit coupling arising first in second order in v/c .

With the laser intensity and ion charge increasing such that second-order effects become important, spin signatures in the dynamics are expected to be visible as noted first recently [23]. For free electrons, similar spin-induced forces have also been noted almost purely analytically, especially most interestingly a small one in the direction of the magnetic field of the laser field [26]. Here, we concentrate on the effect of the spin degree of freedom on bound electron dynamics and radiation in intense laser fields. In this case the used Hamiltonian H_{FW} includes all second-order terms in $1/c^2$ as shown in Eq. (1) of which both the Pauli term H_P and the spin-orbit coupling term contribute to spin effects. As noted in Sec. III A, the Lorentz force may induce a significant angular motion around the ionic core with considerable orbital angular momentum \mathbf{L} with respect to the origin set by the nucleus. We show that the resulting enhanced spin-orbit coupling gives rise to observable effects in the electron dynamics and radiation. In particular, we note a significant splitting of the nonsymmetric bound states due to this additional interaction that leads to well separated doublets and four-line structures in the radiation spectra. In general terms, we understand those also as indications that the influence of the spin and other relativistic effects are both principally observable in experiments and non-negligible in theoretical treatments for relatively low laser intensities.

We are still interested in the weakly relativistic regime of optical laser intensities of up to at about 10^{17} Wcm^{-2} , which have been implemented in several laboratories worldwide and which still allows for laser-bound electron dynamics. We employ the 527-nm (double Nd:glass) laser with an intensity of $7 \times 10^{16} \text{ W/cm}^2$ to interact with $Z=12$ ions, which are

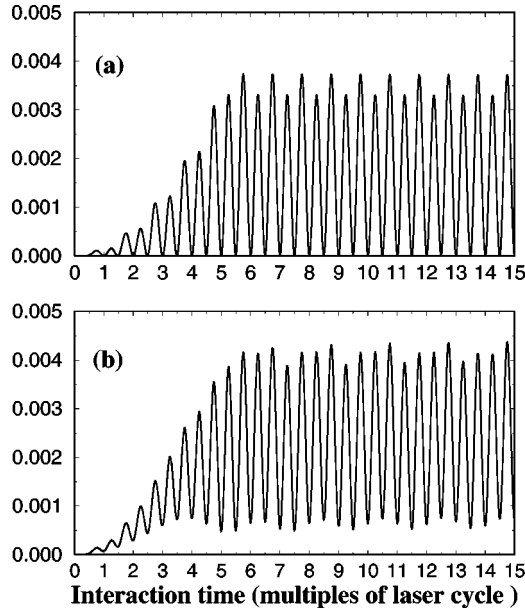


FIG. 10. The dynamics of the spin degree of freedom for the situations without (a) and with (b) spin-orbit interaction as viewed from the population of the wave function with spin-down polarization. The initial electron is spin-up polarized. The intense laser-enhanced spin-orbit coupling leads to an effective spin polarization in the turn-on phase and an additional oscillation due to magnetic field from the nucleus in the rest frame of the electron. The laser parameters involve a wavelength of 527 nm, an intensity of 7×10^{16} W/cm², a 5.25-cycle linear turn-on and a 10-cycle duration with constant amplitude. The parameters for the ionic core are $q_e = 1$, $k = 80.32$ ($Z = 12$ ions).

initially spin-up polarized. The laser pulse has a 5.25-cycle turn-on and 100-cycle constant amplitude duration. In Fig. 10 we address the spin polarization itself and have displayed the expectation value of the electronic wave function in ‘spin-down’ configuration as a function of the interaction time. We compare results from the full second-order Hamiltonian \mathbf{H}_{FW} including spin-orbit coupling with those where spin-orbit coupling \mathbf{H}_{so} has been ignored. Both situations involve a spin flipping with twice the laser frequency. With spin-orbit coupling however the total flipping amplitude is higher because of a second oscillation due to the magnetic field of the frame of reference transformed nucleus \mathbf{B}' . Finally the figure shows an effective polarization due to spin-orbit coupling in the turn-on phase, while without spin-orbit coupling the electron periodically returns to the initial polarization in complete spin-up configuration. Comparing with [23] where a different ion is considered, we see that the dynamics of the spin via the Pauli equation is essentially independent of the nucleus, however, the spin dynamics depends on the charge state of the ion when spin-orbit coupling is included.

The most significant qualitative features appear in the radiation spectrum in terms of strongly laser-enhanced line splitting. In Fig. 11 we have displayed the radiation spectrum of light emitted perpendicular to the plane spanned by the laser polarization and propagation directions and being polarized in x direction. The upper row describes the situation

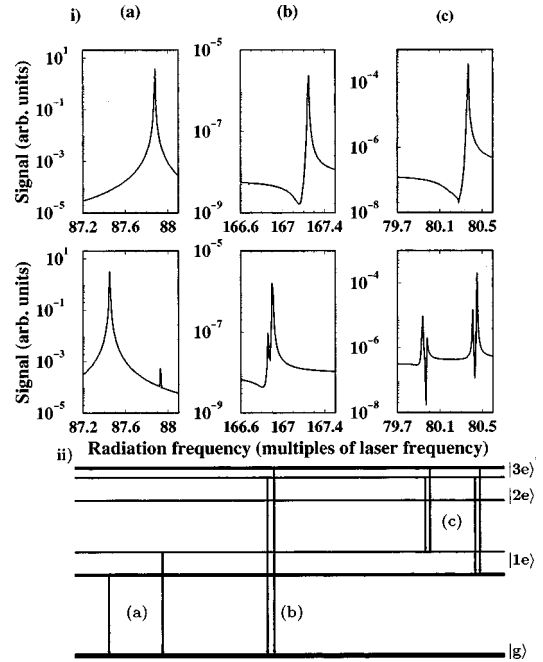


FIG. 11. (i) Radiation spectrum of the laser driven $Z = 12$ ion. The first row corresponds to the Pauli modeled system and the second row is for the case where spin-orbit coupling including the relativistic mass shift and Zitterbewegung is taken into account. (a), (b), and (c) are associated, respectively, with transitions from $|1e\rangle - |g\rangle$, $|3e\rangle - |g\rangle$, and $|3e\rangle - |1e\rangle$ (see also ii). The spectral lines split into doublets [(a) and (b)] and a four-line structure (c) due to the spin-orbit interaction. All parameters are the same as those in Fig. 10 apart from 100 cycles at full strength rather than 10; (ii) The schematic diagram of state splitting as induced by the enhanced spin-orbit interaction due to the intense laser field. We note that asymmetric states split as opposed to symmetric states. Transitions (a), (b), and (c) are associated with the corresponding spectral lines in Fig. 11 (i).

governed by the Pauli Hamiltonian while the lower involves the full second-order Hamiltonian \mathbf{H}_{FW} in Eq. (1). Figures 11(i)(a), 11(i)(b) and 11(i)(c) show the spectral segments corresponding to the resonances of the first excited state $|1e\rangle$ to the ground state $|g\rangle$, the third excited state $|3e\rangle$ with the ground state $|g\rangle$, and the third excited state $|3e\rangle$ to the first excited state $|1e\rangle$. Comparing the upper and lower row we note shifts and splittings of the spectral components into a doublet in (a) and (b) and a four-line structure in (c). In addition, the relativistic Stark redshift is also observable, as discussed at length in Sec. III B. We found also that the Darwin term due to \mathbf{H}_{D} has no notable effects in this situation. We confirmed that the spectral features displayed are generally well separated for ions with different charge states should a possible experiment not allow for a pure sample of the ion of choice.

We explain the doublets and four-line structure with the splitting of the asymmetrical excited states $|1e\rangle$ and $|3e\rangle$ due to the additional spin-orbit interaction as depicted in Fig. 11(ii) while the symmetrical states, possibly s states, remain unchanged. The splitting becomes larger with increasing laser intensity or charge of the ionic core. All transitions give

TABLE I. Dependence of the spin-orbit splitting of the first excited state on the charge state and the laser intensity.

Laser intensity (W/cm ²)	Charge states	
	Z=12	Z=13
3×10^{16}	0.20ω	0.22ω
4×10^{16}	0.25ω	0.29ω
7×10^{16}	0.48ω	0.51ω

rise to spectral features because the common selection rules do not apply in the parameter regime beyond the dipole approximation as investigated here. The bound states in Fig. 11(ii) drawn with thick lines indicate that those states of the split doublet are most populated explaining the relative heights of the spectral lines in Fig. 11(i). The amount of population in the excited states is well above 1% (e.g., 1.25% in the first excited state) such that the total radiation should not be insignificant. We note that the amount of the splitting is $\Delta E/\omega_L \approx 0.48$ for the state $|1e\rangle$ and 0.04 for the state $|3e\rangle$ (here, $\omega_L = 0.0866$ a.u. is the applied laser frequency) so that the enhanced spin-orbit splitting should be easily measurable in experiments. Comparing those values with the amount of spin-orbit splitting without the presence of the laser field, we have evaluated numerically, via the same techniques, $\Delta E_0/\omega_L \approx 0.042$ for $|1e\rangle$ and 0.004 for the state $|3e\rangle$. Thus, we find that the total enhancement factor of the spin-orbit splitting due to the intense laser field for our set of parameters amounts to approximately ≈ 10 . Considering Table I, we find that the spin-orbit splitting increases with higher laser field intensities and for higher charged ions. However, we also emphasize that for less charged ions, in particular hydrogen, spin-orbit coupling has still little significance.

D. Generation of coherent keV x rays

From nonrelativistic laser atom interaction, it is well known that parts of the electronic wave packet, for appropriate parameters, may tunnel through the Coulomb barrier, then propagate essentially freely in the laser field and when returning to the ionic core in the oscillating field may release their energy in form of radiation [8]. The corresponding radiation spectrum in terms of harmonics of the applied field is in fact quite attractive because quite high-frequency coherent light is achievable. Instead of an exponential decay of the spectrum with respect to the harmonic order, we here experience a plateau and a cut-off energy of the emitted harmonics at $I_p + 3.17U_p$. Here I_p is the ionization potential of the ions and $3.17U_p$ the maximal kinetic energy of the electron at the time of return to the nucleus. This law is valid in the tunnel regime where the Keldysh parameter need fulfill $\gamma_K = \sqrt{I_p/2U_p} \ll 1$.

The kinetic energy of electrons increases significantly with the laser intensity. Consequently, higher harmonics are expected with an increasing laser intensity if the ionic potential is raising correspondingly, as shown recently already in the nonrelativistic regime with an output of more than 2000 low-frequency harmonics [36]. We here concentrate on the weakly relativistic regime and show that the harmonic order

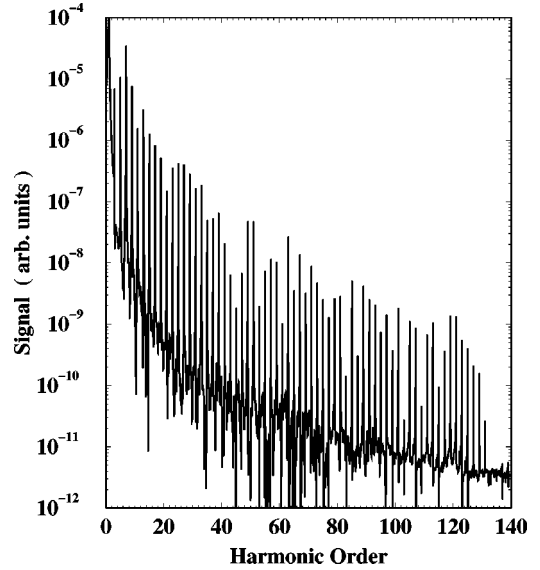


FIG. 12. The harmonic spectrum emitted from $Z=3$ ions with parameters $k=6.48$ and $q_e=1.0$ characterizing the potential. The laser intensity is 2.5×10^{16} W/cm² and the KrF laser wavelength with 248 nm is applied. The laser pulse has a linear 10-cycle turn-on and is followed by a 10-cycle duration with constant amplitude. The 131st harmonic is visible in the the cutoff regime.

increases considerably by enhancing the charge of the ion and simultaneously increasing the laser field. Here we took special care on adapting the ratio of U_p and I_p such that we still remain in the tunneling regime.

In our calculations, we employ the KrF laser (wavelength ~ 248 nm) to interact with multiply charged ions of charge $Z=3$ and $Z=4$. There are two advantages to use short-wavelength lasers: (1) the generated harmonics have a high efficiency and are well separated even near the cutoff because of $\omega_{2n+1} - \omega_{2n-1} = 4\pi/\lambda$ (λ being the fundamental laser wavelength); (2) the numerical resolution is better as the box size is proportional to the square of the laser wavelength and the CPU time to the cube of it. Moreover, the chosen laser wavelength is available in experiments. The pulse envelope is assumed to have a 10-cycle linear turn-on, followed by 10 cycles with constant maximal amplitude. For $Z=3$ ions (potential parameters $k=6.48$, $q_e=1.0$), we use the laser intensity of 2.5×10^{16} W/cm². The result is shown in Fig. 12 in which we find the highest harmonic to be of the 131st order. To the best of our knowledge, the maximum harmonic order ever obtained in experiments for this short driving wavelength is the 37th (last reference in [7]). There the authors expressed that they believe that the He^+ ions may have also contributed to the harmonic emission. Our numerical simulation shows that this harmonic spectrum can be extended to the 131st order if the $Z=3$ ions (Li^{2+}) are employed instead. This harmonic has a wavelength ~ 1.9 nm and the efficiency indicated is still of the level 10^{-10} – 10^{-11} relative to the radiation at the fundamental frequency. Please note in Fig. 12 that we have only shown the radiation polarized in the laser polarization direction as the radiation polarized in the laser propagation direction is relatively small for the parameters chosen here.

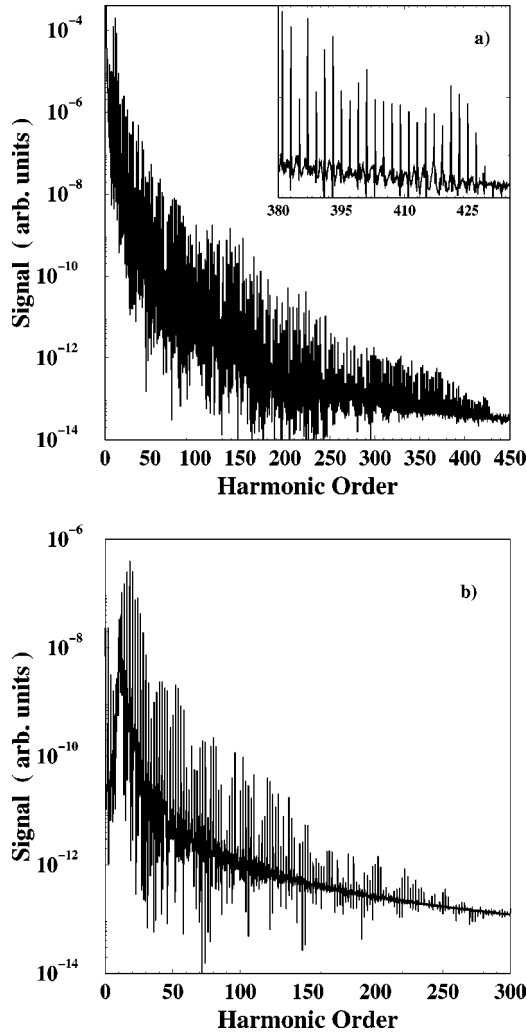


FIG. 13. Same as Fig. 12 but for $Z=4$ ions ($k=10.7$, $q_e=1.0$). The laser intensity is further increased to 10^{17} W/cm² resulting in harmonic emission up to the 427th order with a photon energy well above 2 keV. Consequently coherent keV x rays can be obtained through high harmonic generation with multiply charged ions. The contribution of the harmonic yield in the laser polarization direction is depicted in (a) and the one in the laser propagation direction in (b).

Coherent x rays even in the keV regime can be obtained when $Z=4$ ions (potential parameters $k=10.7$, $q_e=1.0$) are used. In Fig. 13, we display the harmonic spectrum of $Z=4$ ions driven by a laser pulse with the same parameters as in the previous figure but with an intensity of 10^{17} W/cm². The spectrum polarized in the laser polarization direction in (a) has been evaluated via the Fourier transform of $a_x(t)$ and the smaller contribution polarized in the laser propagation direction in (b) via $a_z(t)$ in Eq. (10). The cutoff is enlarged as an inset in the right corner of Fig. 13(a). We emphasize that coherent radiation of the 427th harmonic is clearly observable in spite of the low efficiency of 10^{-13} relative to the radiation at the fundamental frequency. The photon energy of this harmonic exceeds even 2 keV and shall be useful for many applications, e.g., for time-resolved x-ray diffraction. For the parameters chosen, we find no significant deviation

to the cut-off rule even though the factor 3.17 is expected to alter with more than weakly relativistic free electron dynamics changing the kinetic energy at the recollision time. Most remarkably, and unfortunately, the plateau is tilting with increasing charge reducing the efficiency of the highest harmonics substantially. Thus our results indicate that a part of the electronic wave packet can still tunnel through the barrier formed by a deep ionic potential but the amount that tunnels out and returns reduces drastically with the ion charge. Thus with further increasing charge, higher harmonic energies are possible but special care need be devoted to the small efficiency. Coulomb effects are then essential for the tunneled electron wave packet dynamics and solid crystal structures have shown to significantly improve the problem of efficiency (to be presented in subsequent work by our group).

The calculations for Fig. 13 have been carried involving all first order terms in v/c , i.e., including the role of the magnetic field, and the leading terms in $(v/c)^2$. We have chosen parameters in the weakly relativistic regime such that higher terms will not make a difference in the results presented. We note that the spectrum in Fig. 13(a) in fact would look hardly different without all the terms in v/c , however, the one in Fig. 13(b) would hardly resemble the correct one depicted. This is not surprising as the laser induced dynamics in the laser propagation direction is fully induced by the magnetic field component of the laser field.

Regarding experimental possibilities for high harmonics from multiply charged ions in the coherent keV x rays, there are two ways at hand. There may be the double pulse experiment [37] where the first pulse is used to strip several or many electrons of the neutral atoms and then a moderately delayed pulse will interact with the obtained multiply charged ions and generate the coherent keV x rays as described above. However, here the free electrons ionized by the first pulse may influence the phase matching of harmonic emissions and there may also be a mixture of many charge states. The alternative way is to shoot atoms through thin foils, which is clearly a cleaner way to generate ions with a pure charge state [20]. Extremely high densities of multiply charged ions have been generated recently [38], which raises hope for a reasonable efficiency for ion charges well above those investigated here.

E. High-order above-threshold ionization

When laser field strengths are employed that are high with respect to the binding fields of the ionic core, a large part of the electron wave packet will escape the vicinity of the ion and not return. Those electrons may in fact be quite energetic and will be of interest in this section.

We begin by calculating the photoelectron spectrum for $Z=3$ ions with the method described in Sec. II (C). Here, we use a laser pulse with a 3-cycle turn-on, and 10-cycles with constant maximal amplitude. The applied maximal intensity is equal to 2.5×10^{16} W/cm² and the laser wavelength is 248 nm (corresponding to a photon energy near 5 eV). The resulting photoelectron spectrum is displayed in Fig. 14. The spectral range from 860 eV to 900 eV is enlarged as an inset in the right-up corner of this figure. We note very energetic

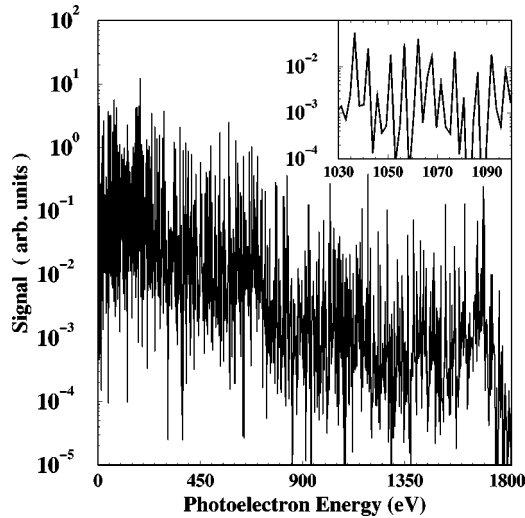


FIG. 14. The photoelectron spectrum for $Z=3$ ions. The laser parameters are the same as those in Fig. 12 but with a steeper turn-on of three cycles. We can observe very energetic (2 keV) photoelectrons and the ATI peaks are spaced by the photon energy even at electron energies close to the order of 1 keV.

electrons with energies up to 2 keV with the usual photon-energy spacing characteristics of photoelectron peaks. Figure 15 shows the case for $Z=4$ ions with an appropriately higher laser intensity of 1.2×10^{17} W/cm². As expected more energetic (above 5 keV) photoelectrons can be detected. A rather regular spacing of the peaks in this above-threshold ionization spectrum is still notable in this keV energy regime.

Thus next to extremely high harmonics we find also very energetic electrons due to above-threshold ionization. In more general terms, these results and the ones in the previous section show that very high-order nonlinear effects are governing the interaction of multiply charged ions with very intense laser fields.

IV. CONCLUSION

We believe to have shown that the physics of multiply charged ions in very intense laser fields is even richer than that for neutral atoms with moderately intense laser fields. There is not merely the effect of scaling the known effects for neutral atoms to the new intensity regime but the upcoming of many relativistic influences imposes a fundamentally different dynamics. We have seen that the magnetic field component of the laser field completely modifies the dynamics and may even induce a partially circular motion around the nucleus with the effect of a reduced expectation value just in the near vicinity of the ionic core. In the regime where second-order terms in v/c are important, the relativistic mass shift modifies clearly the positions of the spectral components in the multiphoton regime. Amplification was found on resonances involving of the order of 100 photons with interesting nondipole spectral features displaced few harmonics away from the atomic resonances. The spin, usually of no importance in the nonrelativistic regime, starts to oscillate

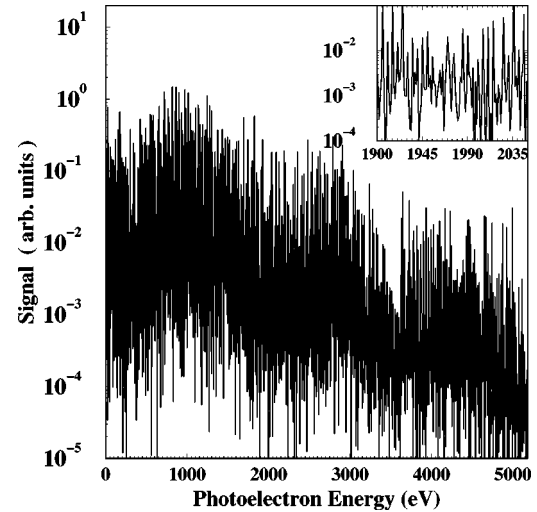


FIG. 15. Similar to Fig. 13 but for $Z=4$ ions. The laser parameters are the same as those in Fig. 14 but involving the higher intensity of 1.2×10^{17} W/cm². More energetic ~ 5 -keV photoelectrons are ejected while conventional ATI features are still conserved.

and via spin-orbit coupling modifies substantially dynamics and radiation. The laser enhanced splitting of resonant spectral lines is a clear relativistic quantum signature.

Those aspects are associated with fundamentally new influences in the weakly relativistic regime with respect to the nonrelativistic case and were most conveniently described by applying the expansion of the Dirac equation up to the second order in v/c . This allowed us to relate each effect to different parts of the Hamiltonian and to carry out our numerical investigations even for the low frequencies available in most present day high power laser systems.

We stressed also that the combination of highly charged ions and high power lasers can be useful for applications. High-order, above threshold, ionization was shown to give rise to photoelectrons in the multi-keV regime already for laser intensities around 10^{17} W/cm². More interestingly, parts of those highly energetic electron wave packets may return to the nucleus and we indicated also coherent high harmonics in the keV regime. Even though for high harmonic generation towards the coherent hard x-ray regime the quantitative aspect appears most attractive, we pointed out also qualitative changes as the problematic tilting of the plateau of the harmonic spectrum with increasing ion charge.

ACKNOWLEDGMENTS

The authors acknowledge funding from the German Research Foundation (Nachwuchsgruppe within Sonderforschungsbereich 276). The hospitality at the Max Planck Institute for complex systems in Dresden where this work was completed is greatly appreciated. S.X.H would like to thank W. Becker for fruitful discussions and acknowledges funding from the Alexander von Humboldt Foundation while in Berlin. C.H.K. acknowledges helpful discussions with M. Casu, J. Ullrich, and M. W. Walser.

- [1] D. Strickland and G. Mourou, *Opt. Commun.* **56**, 219 (1985); P. Maine, *et al.*, *IEEE J. Quantum Electron.* **24**, 398 (1988).
- [2] K. Yamakawa, H. Shiraga, and Y. Kato, *Opt. Lett.* **16**, 1593 (1991); C. Rouyer *et al.*, *ibid.* **18**, 214 (1993); J.P. Chambaret, *et al.*, *ibid.* **21**, 1921 (1996); C.P.J. Barty, *et al.*, *ibid.* **21**, 668 (1996); M.D. Perry, *et al.*, *ibid.* **24**, 160 (1999).
- [3] M. Protopapas, C.H. Keitel, and P.L. Knight, *Rep. Prog. Phys.* **60**, 389 (1997); *Atoms in Intense Laser Fields*, edited by M. Gavrila (Academic, San Diego, 1992); H.R. Reiss, *Prog. Quantum Electron.* **16**, 1 (1992); C.J. Joachain, M. Dörr, and N. Kylstra, *Adv. At. Mol. Phys.* **42**, 225 (2000); T. Brabec and F. Krausz, *Rev. Mod. Phys.* **72**, 545 (2000).
- [4] A.D. Bandrauk, *Molecules in Laser Fields* (Dekker, New York, 1993).
- [5] See, for example, A. McPherson *et al.*, *Nature (London)* **370**, 631 (1994); *Phys. Rev. Lett.* **72**, 1810 (1994); T. Ditmire *et al.*, *ibid.* **75**, 3122 (1995); *Nature (London)* **386**, 54 (1997); **398**, 489 (1999).
- [6] M.D. Perry and G. Mourou, *Science* **264**, 917 (1994); P.A. Norreys *et al.*, *Phys. Rev. Lett.* **76**, 1832 (1996).
- [7] B.W. Shore and P.L. Knight, *J. Phys. B* **20**, 413 (1987); W. Becker, S. Long, and J.K. McIver, *Phys. Rev. A* **41**, 4112 (1990); **50**, 1540 (1994); A. L'Huillier and P. Balcou, *Phys. Rev. Lett.* **70**, 774 (1993); J.J. Macklin, J.D. Kmetec, and C.L. Gordon III, *Phys. Rev. Lett.* **70**, 766 (1993); S.G. Preston *et al.*, *Phys. Rev. A* **53**, R31 (1996).
- [8] P.B. Corkum, *Phys. Rev. Lett.* **71**, 1994 (1993); J.L. Krause, K.J. Schafer, and K.C. Kulander, *ibid.* **68**, 3535 (1992); M. Lewenstein *et al.*, *Phys. Rev. A* **49**, 2117 (1994); M. Protopapas *et al.*, *ibid.* **53**, R2933 (1996); G. van de Sand and J.M. Rost, *Phys. Rev. Lett.* **83**, 524 (1999); M.W. Walser *et al.*, *ibid.* **85**, 5082 (2000); R.M. Potvliege, N.J. Kylstra, and C.J. Joachain, *J. Phys. B* **33**, L743 (2000); D.B. Milošević, S.X. Hu, and W. Becker, *Phys. Rev. A* **63**, 011403(R) (2001); K.Z. Hatsagortsyan and C.H. Keitel, *Phys. Rev. Lett.* **86**, 2277 (2001).
- [9] Ch. Spielmann *et al.*, *Science* **278**, 661 (1997); M. Schnürer *et al.*, *Phys. Rev. Lett.* **80**, 3236 (1998); Ch. Spielmann *et al.*, *IEEE J. Sel. Top. Quantum Electron.* **4**, 249 (1998); G. Tempea, M. Geissler, and T. Brabec, *J. Opt. Soc. Am. B* **16**, 669 (1999); G. Tempea *et al.*, *Phys. Rev. Lett.* **84**, 4329 (2000).
- [10] Z. Chang *et al.*, *Phys. Rev. Lett.* **79**, 2967 (1997); H. Kapteyn and M. Murnane, *Phys. World* **12**, 31 (1999); S. G. Durfee III *et al.*, *Phys. Rev. Lett.* **83**, 2187 (1999); R. Barfels *et al.*, *Nature (London)* **406**, 164 (2000).
- [11] P. Agostini *et al.*, *Phys. Rev. Lett.* **42**, 1127 (1979); R.R. Freeman *et al.*, *ibid.* **59**, 1092 (1987).
- [12] Q. Su, J.H. Eberly, and J. Javanainen, *Phys. Rev. Lett.* **64**, 862 (1990); V.C. Reed, P.L. Knight, and K. Burnett, *ibid.* **67**, 1415 (1993).
- [13] J. Grochmalicki, M. Lewenstein, and K. Rzazewski, *Phys. Rev. Lett.* **66**, 1038 (1991); T. Katsouleas and W.B. Mori, *ibid.* **70**, C1561 (1993); C.H. Keitel and P.L. Knight, *Phys. Rev. A* **51**, 1420 (1995); J.R. Vázquez de Aldana and Luis Roso, *Opt. Express* **5**, 144 (1999); V.P. Krainov, *J. Phys. B* **32**, 1607 (1999); R.M. Potvliege, *Laser Phys.* **10**, 143 (2000); H.R. Reiss, *Phys. Rev. A* **63**, 13409 (2000); N.J. Kylstra *et al.*, *Phys. Rev. Lett.* **85**, 1835 (2000).
- [14] C.H. Keitel, P.L. Knight, and K. Burnett, *Europhys. Lett.* **24**, 539 (1993); N.J. Kylstra, A.M. Ermolaev, and C.J. Joachain, *J. Phys. B* **30**, L449 (1997); C.H. Keitel *et al.*, *ibid.* **31**, L75 (1998); C. Szymanowski, C.H. Keitel, and A. Maquet, *Laser Phys.* **9**, 133 (1999); J.C. Czesznegi, G.H. Rutherford, Q. Su, and R. Grobe, *ibid.* **9**, 41 (1999); R.E. Wagner, R.J. Reverly, Q. Su, and R. Grobe, *Phys. Rev. A* **60**, 3233 (1999).
- [15] U.W. Rathe, C.H. Keitel, M. Protopapas, and P.L. Knight, *J. Phys. B* **30**, L531 (1997); C. Szymanowski *et al.*, *Phys. Rev. A* **56**, 3846 (1997); J.W. Braun, Q. Su, and R. Grobe, *ibid.* **59**, 604 (1999).
- [16] K.W.D. Ledingham, *et al.*, *Phys. Rev. Lett.* **84**, 899 (2000); G. Pretzler *et al.*, *Phys. Rev. E* **58**, 1165 (1998); T.E. Cowan *et al.*, *Phys. Rev. Lett.* **84**, 903 (2000).
- [17] C.I. Moore, J.P. Knauer, and D.D. Meyerhofer, *Phys. Rev. Lett.* **77**, 2335 (1996); S.J. McNaught, J.P. Knauer, and D.D. Meyerhofer, *Phys. Rev. A* **58**, 1399 (1998); C. Bula *et al.*, *Phys. Rev. Lett.* **76**, 3116 (1996); S.Y. Chen, A. Maksimchuk, and D. Umstadter, *Nature (London)* **396**, 653 (1998).
- [18] L.S. Brown and T.W. Kibble, *Phys. Rev.* **133**, A705 (1964); E.S. Sarachik and G.T. Schappert, *Phys. Rev. D* **1**, 2738 (1970); A.I. Nikishov and V.I. Ritus, *Zh. Éksp. Teor. Fiz.* **46**, 776 (1966) [*Sov. Phys. JETP* **19**, 529 (1964)]; I.I. Goldman, *ibid.* **46**, 1412 (1964) [**19**, 954 (1964)].
- [19] D.J. Urbach and C.H. Keitel, *Phys. Rev. A* **61**, 043409 (2000).
- [20] P.H. Hokler and Th. Stoehlker, *Adv. At., Mol., Opt. Phys.* **37**, 297 (1996); J. Ullrich *et al.*, *J. Phys. B* **30**, 2917 (1997); J.R. Crespo López-Urrutia *et al.*, *Hyperfine Interact.* **127**, 497 (2000).
- [21] E.M. Snyder *et al.*, *Phys. Rev. Lett.* **77**, 3347 (1996); T. Ditmire *et al.*, *ibid.* **78**, 2732 (1997); *Phys. Rev. A* **57**, 369 (1998).
- [22] S.X. Hu and C.H. Keitel, *Europhys. Lett.* **47**, 318 (1999).
- [23] S.X. Hu and C.H. Keitel, *Phys. Rev. Lett.* **83**, 4709 (1999).
- [24] L.L. Foldy and S.A. Wouthuysen, *Phys. Rev.* **78**, 29 (1950).
- [25] Paul Strange, *Relativistic Quantum Mechanics* (Cambridge University Press, Cambridge, 1998).
- [26] M.W. Walser and C.H. Keitel, *J. Phys. B* **33**, L221 (2000); M.W. Walser, C. Szymanowski, and C.H. Keitel, *Europhys. Lett.* **48**, 533 (1999).
- [27] K.C. Kulander *et al.*, in *Proceedings of the Workshop on Super-Intense Laser Atom Physics (SILAP)*, edited by B. Piraux (Plenum, New York, 1993).
- [28] J.H. Eberly, Q. Su, and J. Javanainen, *Phys. Rev. Lett.* **62**, 881 (1989).
- [29] M.R. Hermann and J.A. Fleck, Jr., *Phys. Rev. A* **38**, 6000 (1988); S.X. Hu and Z.Z. Xu, *ibid.* **56**, 3916 (1997); S.X. Hu, W.X. Qu, and Z.Z. Xu, *ibid.* **57**, 3770 (1998).
- [30] M.D. Feit, J.A. Fleck, Jr., and A. Steiger, *J. Comput. Phys.* **47**, 412 (1982).
- [31] J.L. Krause, K.J. Schafer, and K.C. Kulander, *Phys. Rev. A* **45**, 4998 (1992); S.X. Hu, W.X. Qu, and Z.Z. Xu, *J. Phys. B* **31**, 1523 (1998).
- [32] R.W. Heather, *Comput. Phys. Commun.* **63**, 446 (1991); S.X. Hu, W.X. Qu, and Z.Z. Xu, *Appl. Phys. Lett.* **73**, 2552 (1998).
- [33] M. Protopapas, C.H. Keitel, and P.L. Knight, *J. Phys. B* **29**, L591 (1996).
- [34] R. Taïeb, V. Véniard, and A. Maquet, *Phys. Rev. Lett.* **81**, 2882 (1998).

- [35] O. Latinne, C.J. Joachain, and M. Dörr, *Europhys. Lett.* **26**, 333 (1994); J.R. Vázquez de Aldana and Luis Roso, *J. Phys. B* **33**, 3701 (2000).
- [36] M. Casu, C. Szymanowski, S.X. Hu, and C.H. Keitel, *J. Phys. B* **33**, L411 (2000); see also, S. E. Harris, *Phys. Rev. Lett.* **31**, 341 (1973); S. Kubodera *et al.* *Phys. Rev. A* **48**, 4576 (1993).
- [37] For example, J. Zhang *et al.*, *Science* **276**, 1097 (1997).
- [38] S. Debosh *et al.*, *Zh. Éksp. Teor. Fiz.* **88**, 2051 (1999) [*JETP* **115**, 1122 (1999)]; G.V. Ivanenkov *et al.*, *ibid.* **114**, 1216 (1998) [**87**, 663 (1998)].